ORNL/TM-2023/3045

Report on FY 2023 Welding R&D at ORNL in Support of ASME Alloy 709 Code Case Development

Zhili Feng
Yiyu Wang
Jack Ward
Yanli Wang

September 2023

OAK RIDGE National Laboratory

ORNL IS MANAGED BY UT-BATTELLE LLC FOR THE US DEPARTMENT OF ENERGY

ORNL/TM-2023/XXX

Materials Science and Technology Division

REPORT ON FY 2023 WELDING R&D AT ORNL IN SUPPORT OF ASME ALLOY 709 CODE CASE DEVELOPMENT

Zhili Feng
Yiyu Wang
Jack Ward
Yanli Wang

September 2023

Prepared by
OAK RIDGE NATIONAL LABORATORY
Oak Ridge, TN 37831
managed by
UT-BATTELLE LLC
for the
US DEPARTMENT OF ENERGY
under contract DE-AC05-00OR22725

This page intentionally left blank.

CONTENTS

LIST OF FIGURES

LIST OF TABLES

ACRONYMS

ART	Advanced Reactor Technologies
ASME	The American Society of Mechanical Engineers
ASTM	American Society for Testing and Materials. (aka, ASTM International)
DOE	Department of Energy
ESR	Electroslag Remelting
FR	Fast Reactors
FL	Fusion Line
GTAW	Gas Tungsten Arc Welding
HAZ	Heat Affected Zone
ORNL	Oak Ridge National Laboratory
SFR	Sodium Fast Reactor
SRF	Stress Reduction Factors
SA	Solution Annealed

ACKNOWLEDGMENT

This research was sponsored by the United States (U.S.) Department of Energy (DOE) under Contract No. DE-AC05-00OR22725 with Oak Ridge National Laboratory (ORNL), which is managed and operated by the UT– Battelle LLC. Programmatic direction was provided by the Office of Nuclear Reactor Deployment of the DOE Office of Nuclear Energy.

The authors gratefully acknowledge the support provided by Sue Lesica of DOE-NE, Federal Materials Lead for the Advanced Reactor Technologies (ART) Program; Kaatrin Abbott of DOE-NE, Federal Manager, ART Fast Reactor Program (FRP); Bo Feng of Argonne National Laboratory, National Technical Director, ART FRP; and T.-L. Sham of Idaho National Laboratory, Technology Area Lead, Advanced Materials, ART Program.

The authors also wish to thank ORNL staff members Jeremy Moser and Brad Hall for carrying out the experiments on mechanical properties. The time spent by Lianshan Lin and Jian Chen of ORNL reviewing this report is acknowledged.

ABSTRACT

As part of the Alloy 709 (A709) ASME Code Case development effort under the Advanced Reactor Technologies (ART) Program, this work covers the development of the technical basis for weld fabrication and weld qualification of A709. This report summarizes the A709 welding research conducted at Oak Ridge National Laboratory (ORNL) in FY 2023.

One of the focuses of the A709 welding research at ORNL is to relax the restriction of the P content in the A709 filler metal weld wire. In this report, we show the success in welding of high phosphorus (P) commercial A709 plates using A709 weld wires with relaxed P content of 80 wppm. A test weld was fabricated with the 80 wppm weld wire on the first commercial heat A709 base metal with 140 wppm P content using gas tungsten arc welding (GTAW). The test weld passed all weld qualification tests without issues. This study concludes that A709 matching filler metal with moderate amount of P of less than 80 wppm could be used to produce code qualified A709 welds with standard welding process without special treatment. It is recommended that the P level in the weld wire to be kept low to avoid hot cracking.

Cross-weld specimens were machined from the two A709 production welds.. Cross welding creep rupture Code Case testing on these two production welds was initiated . The preliminary cross-weld creep tests results continue to show little or no creep strength reduction relative to the base metal.

1. INTRODUCTION

Alloy 709 (A709) is an advanced nitrogen-stabilized and niobium-strengthened austenitic stainless steel. Compared to a reference construction material 316H stainless steel for sodium fast reactor (SFR), A709 has enhanced creep strength, good steam oxidation resistance and hot corrosion resistance. It is an attractive candidate construction material for SFR, and was recommended as a Class A structural material through a DOE-NE ART material down-selection and intermediate-term testing program. A comprehensive Code qualification plan was developed to generate the data package and to develop material-specific design parameters required for Class A component design in ASEM Section III, Division 5 (Sham, et al., 2022).

In collaboration with two US steel fabricators, DOE-NE ART program successfully scaled up the production of Alloy 709 (A709) in plate form from a laboratory heat of 500 lb to three commercial heats of the A709 with the commercial Heat-1 of ~45,000 lb, commercial Heat-2 of ~41,000 lb, and commercial Heat-3 of ~38,000 lb. The commercial Heat-1 plates were fabricated by G.O. Carlson Inc of Pennsylvania, whereas the second and third heats were both fabricated by Allegheny Technologies Incorporated (ATI). The three commercial heats of A709 base metal were produced by argon-oxygen-decarburization (AOD) followed by electroslag remelted (ESR).

Welding is essential in construction of high temperature reactor structure components. The Code Case qualification of A709 would require the development of a sound technical basis for welding. It would include the development of welding guidelines with supporting testing results to fabricate ASME Section IX (ASME, 2019) qualified welds using weld wires with appropriately specified chemistry range, to eliminate solidification cracking, minimize stress relaxation cracking susceptibility, and retain the good high temperature mechanical properties, for selected heats meeting relevant ASTM/ASME chemistry specifications.

A709 is derived from NF709, i.e., TP310MoCbN (UNS S31025) specified in ASME BPVC.II SA-213/SA-213M (ASME, 2021). NF709 seamless tube was developed by Nippon Steel Corporation in Japan for boiler tubing applications. Previous studies such as these by Nippon Steel (2013), suggested that

NF709 has relatively good weldability. A709 filler metal and Alloy 625 filler metal were the two weld metals that Nippon Steel had recommended to weld seamless tubing. Performance of A709 weldment fabricated using Alloy 625 filler metal in sodium was found to be less than optimal during the A709 intermediate term testing program because of the high solubility of nickel in sodium. Weldment fabricated from A709 filler metal (the so-called matching filler metal) was found to have good sodium compatibility. However, earlier welding studies on experimental heats of A709 in plate form by the ART Program (Yamamoto, 2014) revealed potential issues of weld solidification cracking when the level of impurities such as P is high but still within the ASME BPVC.II SA-213/SA-213M (ASME, 2021). Only the weldment with very low P content (less than 20 wppm, or <0.002 wt.%) *in both the base metal (plate form) and the matching filler metal* passed the ASME Section IX weldment qualification test. While a Section IX qualified weldment was fabricated successfully, the requirement of very low P content (20 wppm) places a severe restriction.

Computational modeling with Scheil simulations of non-equilibrium solidification found that P has the most important impact on solidification behavior. Increasing levels of P from 0.002 wt.% (20 wppm) to 0.018 wt. % (180 wppm) led to a decrease in the solidus temperature of over 300 °C (Feng, Vitek, Liu, & Wang, 2018). The modeling results lead to the development of strategies to weld A709 having wide range of chemistries without weld solidification cracking to support code qualification. One of the approaches was to limit the P level of the weld wire when welding A709 base metal having relatively high P. For weld wires with high P levels, special welding procedures or innovative welding techniques may be necessary to produce code qualified welds.

A series of ASME Section IX qualified welds were successfully fabricated using the low P weld wire (<20 wppm P) on the first commercial heat (Heat 58776) A709 plates (Feng et al. 2019, 2020, 2021, 2022), including the two production welds. Through welding parameters optimization, ORNL demonstrated the possibility of welding the Heat 58776 plates using high P weld wire (140 wppm P), although welding defects related to solidification cracking within the qualified limit could not be eliminated (Feng et al. 2019). It is noted that this heat A709 plates has relatively high P level of 140 wppm. To this end, one of the focuses of the A709 welding research at ORNL is to relax the restriction of the P content in the A709 filler metal weld wire (Feng et al. 2019, 2020, 2021, 2022).

In FY 2023, the study on the P content restriction in the A709 weld wire has been completed, and we report the success in fabrication of Code qualified A709 with relaxed P content of 80 wppm for the weld wire. Additionally, the status of the ongoing A709 cross-weld Code Case testing is updated in this report.

2. MATERIALS AND SPECIMENS

2.1 ALLOY 709 BASE METAL PLATES

In this report, the base metal plates used for the A709 welding research were from commercial Heat-1 (Carlson heat), and commercial Heat-2 fabricated by ATI. The as-received plates were hot rolled, and solution annealed at a minimum temperature 1150 °C. The plates from the two heats received an additional heat treatment: 775 °C for 10 hours in air, followed by air cooling, following the heat treatment protocol by Zhang, Sham and Young, (2019).

Table 1 summarized the two A709 base metal plates with the heat number 58776 and 529900 used in this study. The chemical compositions of listed in Table 1 are the remelted product for the Carlson heat and product chemistry analysis for the ATI heat. The chemical compositions of these two base metal plates are listed in Table 2. For comparison, the specifications for the chemical requirements of NF709, TP310MoCbN, seamless tubing, with a UNS number of S31025 in ASME SA-213 (ASME, 2021) are

also listed in Table 2. Both commercial heats met the specified NF709 chemical requirements. As shown in the table, the Carlson heat has relatively high P level at 0.014 wt. % (140 wppm) and ATI heat has lower P level of 0.003 wt.% (30 wppm)

Table 1. Commercial heats of A709 base metal plates for A709 weldments

Material	Commercial Heat-1	Commercial Heat-2
Fabricator	G.O. Carlson Inc	Allegheny Technologies Incorporated
Master heat number	58776	529900
Base metal Plate ID	58776-3RBC1	CG05454
Plate gage (in)	1	2
Measured plate thickness, (in)	1.125	2.05
Plate Solution Heat Treatment, (°C)	1150	1150
Aging Heat Treatment	775 °C, 10 h, air cool	775 °C, 10 h, air cool

Table 2. Chemical compositions of the two commercial heat A709 base metal plates (wt %).

Element	Commercial Heat 1 (Plate 58776-3RBC1)	Commercial Heat 2 (Plate CG05454)	ASME SA-213 UNS-S31025 Specification
	(wt.%)	**(wt.%)**	**(wt.%)**
C	0.066	0.08	0.10 max
Cr	20.05	19.9	19.5–23.0
Co	0.02	0.02	–
Ni	25.14	24.6	23.0–26.0
Mn	0.9	0.9	1.50 max
Mo	1.51	1.5	1.0–2.0
N	0.152	0.15	0.10–0.25
Si	0.38	0.39	1.00 max
P	0.014	0.003	0.030 max
S	0.001	<0.001	0.030 max
Ti	0.01	<0.01	0.20 max
Nb	0.26	0.17	0.10–0.40
Al	0.02	0.02	–
B	0.003	0.004	0.002–0.010
Cu	0.06	0.06	–
Fe	Balance	Balance	Balance

2.2 ALLOY 709 FILLER METAL WELD WIRES

Previous computational solidification simulation modeling with Scheil simulations of non-equilibrium solidification found that P has the most important impact on solidification behavior. Increasing levels of P from 0.002 wt.% (20 wppm) to 0.018 wt.% (180 wppm) led to a decrease in the solidus temperature of

over 300°C (Feng, Vitek, Liu, & Wang, 2018). That is, high levels of P lead to very large increases in the non-equilibrium solidification temperature range. Thus, P is expected to significantly increase the susceptibility of weld solidification cracking of A709. This conclusion was supported by limited experimental data that showed poor weldability and considerable cracking for experimental A709 heats (< 20 wppm P) when welded with weld wires of high P levels (Yamamoto, 2014,), although optimizing and carefully control of the welding parameters could result in improved weld quality and pass the ASME Section IX qualification tests (Feng, et al., 2020). Therefore, in addition to the development of code qualified A709 welds, another focus of the A709 welding research at ORNL is to relax the restriction of the P content.

To experimentally investigate the effect of P content in the A709 weld wire filler metal, A709 weld wires were fabricated using base metals with different levels of P through a wire cold drawing process. In our previous study, the P content in the weld wire was relaxed from <20 wppm to ~30 wppm, demonstrated through the fabrication of Code qualified weld using standard GTAW process (Feng, et al., 2022). In FY23, a new heat of A709 weld wire with nominal P content of 80 wppm was fabricated to further evaluate the possibility of further relaxing the P restriction in the weld wire.

The supply material for this new A709 weld wire was the third commercial heat A709 plate fabricated by ATI Specialty Rolled Products. The heat number is 530843 and plate ID is CG45192. The A709 weld wire was fabricated through a wire cold drawing process.

Table 3 lists the chemical compositions of the 4 A709 weld wires used for the A709 welding reserach at ORNL. All the weld wires used meet the specified NF709 chemical requirements. The P levels in weld wires are 140 wppm P from Heat 58776-4A, 30 wppm Heat 529900, < 20 wppm P from lab Heat 011367-08, and 80 wppm from Heat 530843.

Table 3. Chemical compositions of plates for fabrication of Alloy 709 weld wires (wt.%).

A709 weld wires	A709 wire-140wppm	A709 wire <20wppm	A709 wire 30wppm	A709 wire 80wppm	ASME SA-213 UNS-S31025 Specification
	Heat No. 58776-4A	Heat No. 011367-08	Heat No. 529900	Heat No. 530843	
C	0.07	0.079	0.08	0.07	0.10 max
Cr	19.93	20.03	19.9	19.8	19.5–23.0
Co	0.02	<0.01	0.02	0.01	–
Ni	24.98	25.05	24.6	25	23.0–26.0
Mn	0.91	0.87	0.9	0.9	1.50 max
Mo	1.51	1.48	1.5	1.5	1.0–2.0
N	0.148	0.156	0.15	0.15	0.10–0.25
Si	0.44	0.28	0.39	0.44	1.00 max
P	**0.014**	**<0.002**	**0.003**	**0.008**	**0.030 max**
S	<.001	<0.0013	<0.001	0.001	0.030 max
Ti	0.04	<0.01	<0.01	<0.01	0.20 max
Nb	0.26	0.28	0.17	0.18	0.10–0.40
Al	0.02	0.02	0.02	0.02	–
B	0.0045	0.003	0.004	0.005	0.002–0.010
Cu	0.06	<0.01	0.06	0.04	–
Fe	Balance	Balance	Balance	Balance	Balance

2.3 ALLOY 709 WELD GEOMETRY AND TEST SPECIMENS

Single V groove with 20° bevel was the geometry used for welding of the base metal plates which had nominal thickness of 1.125 in and. Double-V groove was used for the for welding of the base metal plates with nominal thickness of 2.05 in (Feng et al., 2022). They are shown in Figure 1.

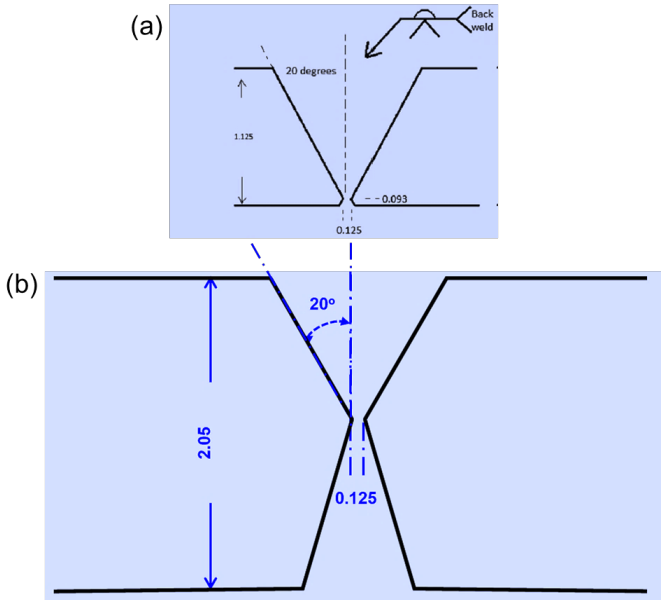

Figure 1. Single V-groove joint and double V preparation details used in the study.
Dimensions are in inches.

Room temperature cross-weld tensile tests are required per welding procedure qualifications requirements in ASME Section IX. The tensile specimen geometry and dimensions for A709 welds are shown in Figure 2. Two sets of tensile tests were performed on each weld for evaluation of the room temperature properties. For the welds with plate thickness of about 1-in, each set of the tensile tests include two specimens, whereas the thicker weld with ~2-in thickness had 4 tensile specimens each set at one cross-section, as schematically shown in

Figure 3. The centerline of the weldment is at the mid-length of the gage section, and the entire weld was within the reduced section of the tensile specimen.

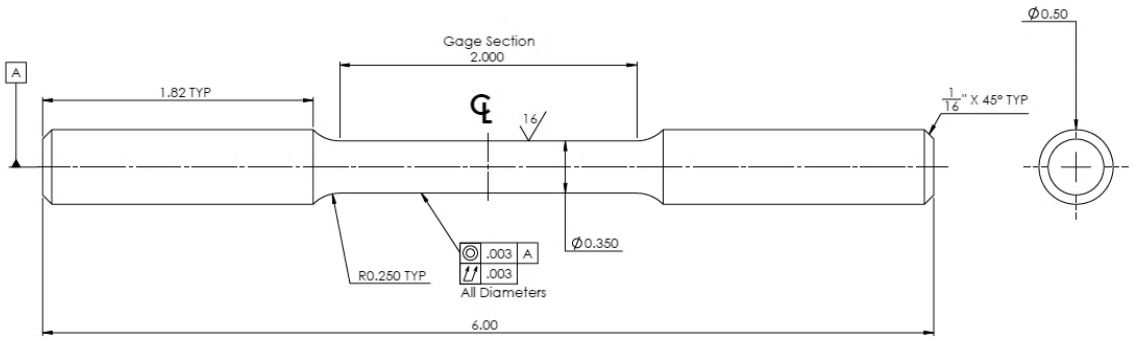

Figure 2. Room temperature cross-weld tensile specimen geometry.
Dimensions are in inches.

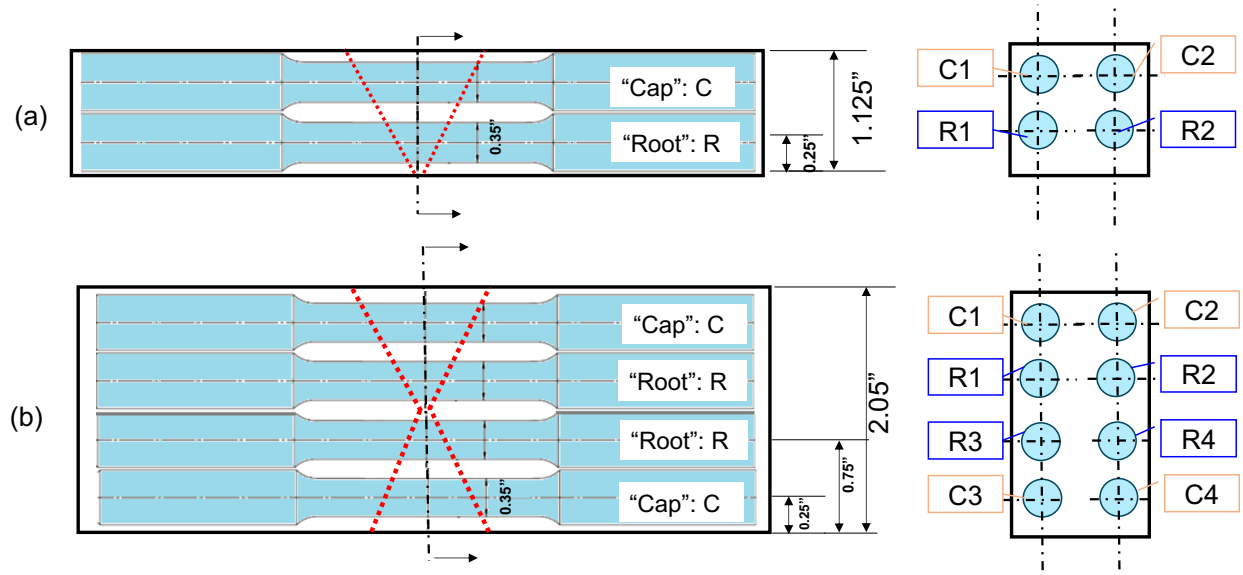

Figure 3. Schematics of the locations of the cross-weld weld tensile specimens

In support of A709 code qualification, cross-weld creep testing is also tasked under this welding research program. The weld creep specimen used the same geometry as the base metal creep specimen, shown in Figure 4.

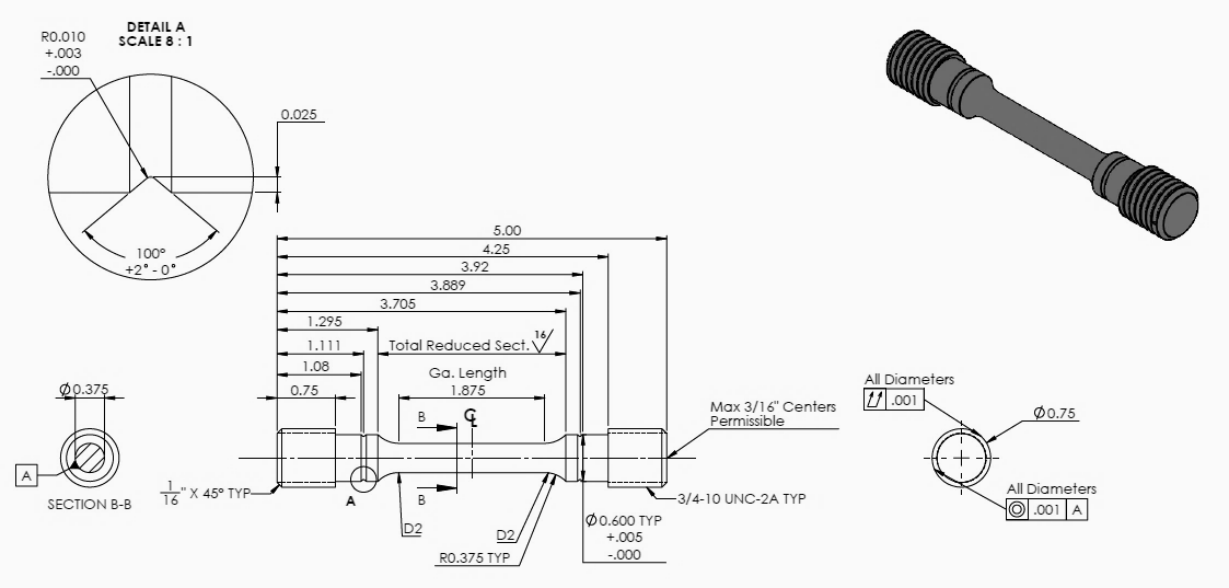

Figure 4. Alloy 709 cross-weld creep specimen geometry
Dimensions are in inches.

For A709 cross-weld Code Case testing, one cross-weld creep specimen was machined in the thickness direction of the 1-in plate welds and two from the 2-in plate weld, as shown in Figure 5. The cross-weld creep specimens are machined to allow the centerline of the weldment at the mid-length of the gage section, and the entire weld was within the reduced section of the tensile specimen.

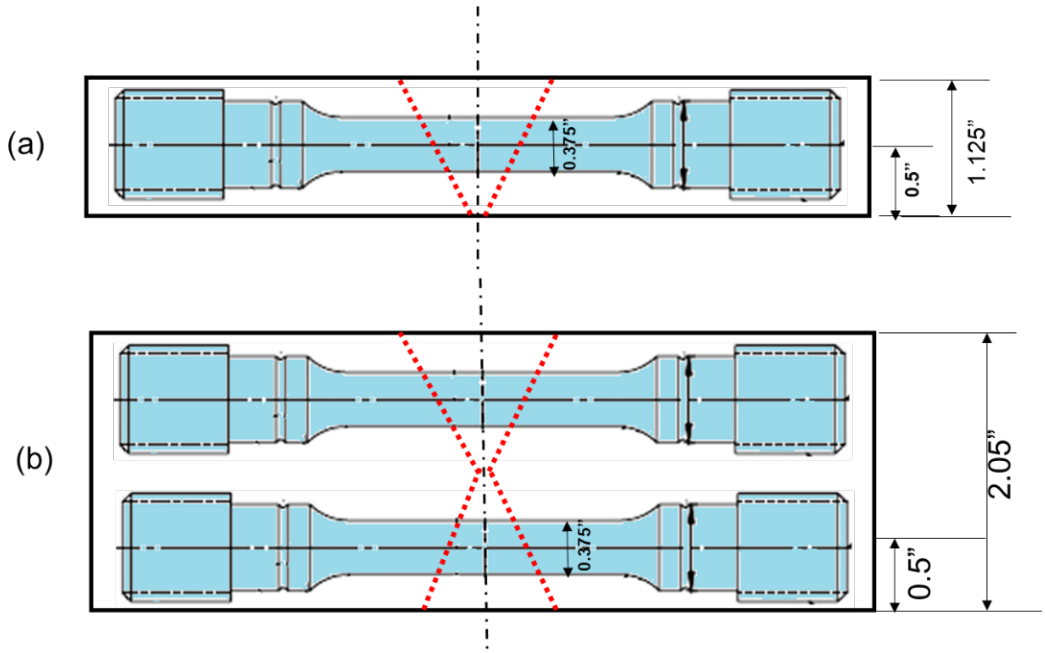

Figure 5. Schematics of the location of the cross-weld weld creep specimens.
Dimensions are in inches. The red lines represent the fusion line.

3. RELAXING THE RESTRICTION OF P LEVEL IN ALLOY 709 WELD WIRE

3.1 ALLOY 709 WELD W14 AND QUALIFICATION TESTING

In an effort of relaxing the restriction of the P content in the A709 weld wire, a new weld wire was fabricated from plate CG45192 with nominal 80 wppm of P (Heat No. 530843). A test weld W14 was fabricated with this new weld wire on the first commercial heat plates with high P content of 140 wppm using GTAW process.

A photograph of this weld is shown in Figure 6. The weld W14 was inspected with X-ray (Figure 7) and found acceptable per ASME Section IX with no relevant indications of welding flaws. Table 4 has summarized the critical information about this weld W14.

Weld 14 was further evaluated with side bending tests and tensile tests at room temperature. The results from three duplicate side bend tests showed no indications of any cracks in the weldment, as shown in Figure 8. Two sets of cross-weld tensile test specimens were machined from Weld W14. Each set of the tensile tests had one specimen out of the cap of the weld, C1 and C2, and one out of the region close to the root of the weld, R1 and R2. The room temperature tensile stress-strain curves are plotted in Figure 9. The tensile strengths of the four test specimens are summarized in Table 5. The tensile strengths of all four specimens were above the minimum ASME code required base metal tensile strength of 640 MPa. For both sets of the tensile tests, the root of the weld consistently showed higher tensile strength than the cap of the weld.

Figure 6. Photograph of W14 Weld.

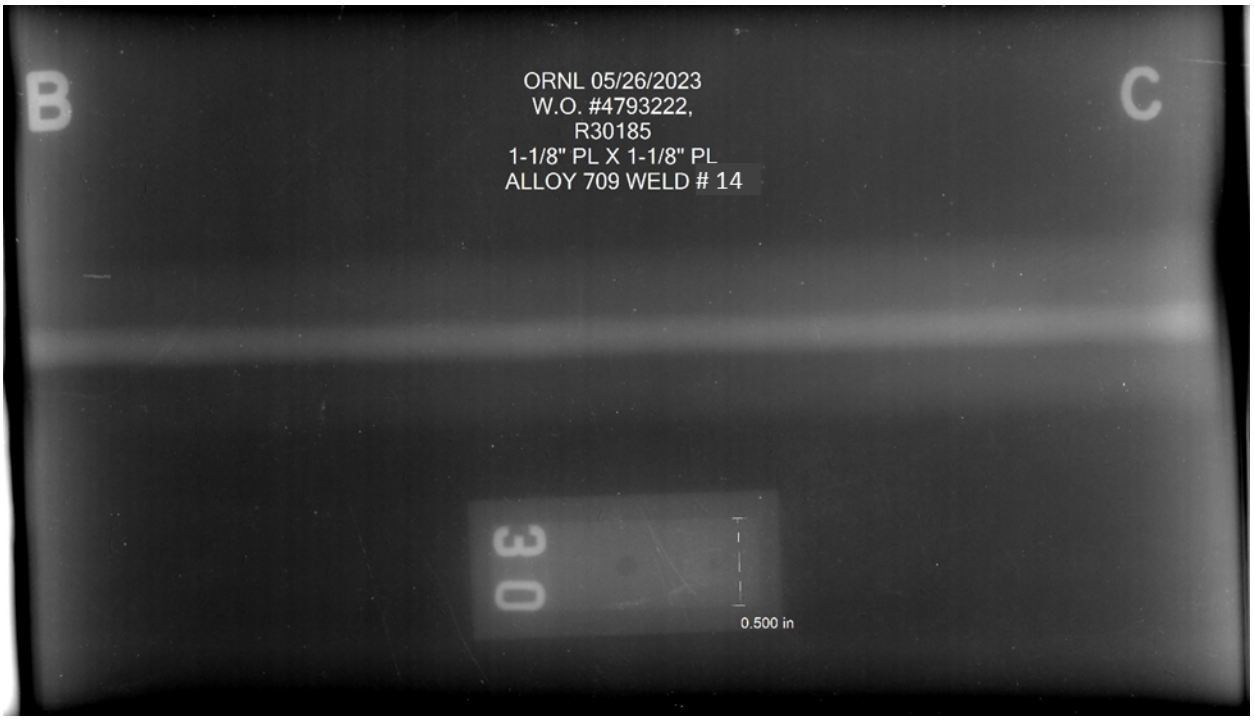

Figure 7. Radiographic inspection (X-ray testing) of W14 Weld.

Table 4. Alloy 709 Weld W14

Alloy 709 welds		**Weld 14**
Weld Wire	**P Level (wppm)**	**80**
	Heat No. of the supply material for weld wire	X-ray
	Wire dia. (in)	0.035
Base Metal Plate		Commercial heat-plate (Heat No 58776)
Base metal plate thickness (in)		1.12
Total weld length (in)		15
Weld joint geometry		20° single V
ASME Sec. IX Weld Qualification	**X-Ray**	Pass
	Side Bend	Pass
	RT Tensile	Pass

Figure 8. Photographs of the side-bend specimens after testing (W14)

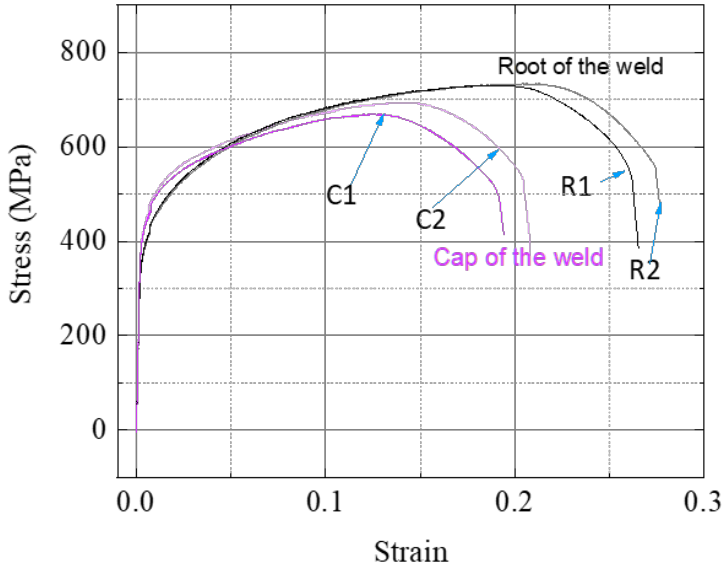

Figure 9. Room temperature cross-weld tensile results for Alloy 709 weld W14.

Table 5. Room temperature cross-weld tensile results for Weld W14

Location of the tensile specimens	Tensile strength, (MPa)
Cap of the weld 1	669.4
Cap of the weld 2	694.1
Root of the weld 1	729.8
Root of the weld 2	733.6

A photograph of the specimens after tensile tests is shown Figure 10. The center of the weldment was marked with an arrow. All 4 tensile specimens failed inside the weldment, and the failure mode is ductile. Note that, the surface paint speckles on these specimens were used for Digital Imaging Correlation (DIC) analysis.

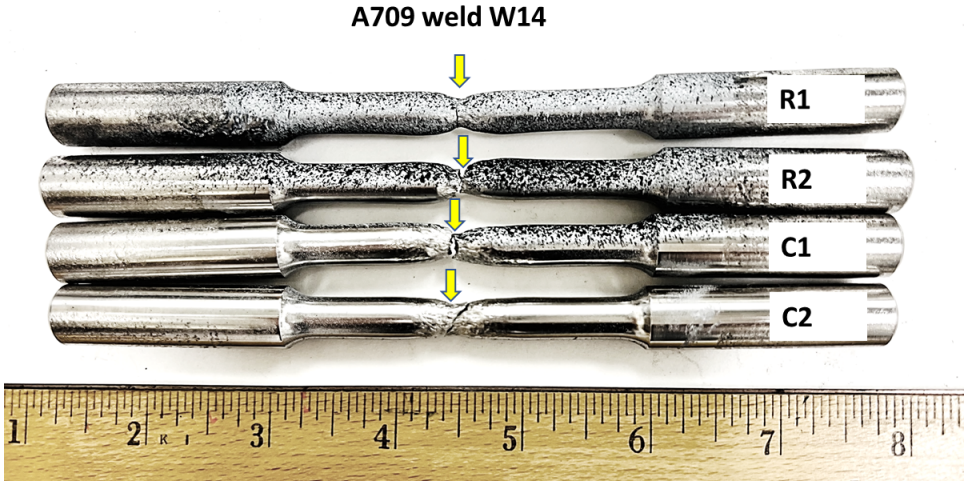

Figure 10. Photograph of the tested cross-weld tensile specimens from production weld W14

As such, weld W14 passed the ASME Section IX weld quality requirement without issues. This study concludes the success in further relaxing the P content in the A709 weld wire to 80 wppm. The P content will be re-measured in future for more accurate description.

To understand the deformation behavior of the W14 cross-weld under tensile test, the full field tensile strain maps from Digital Image Correlation (DIC) are presented in Figure 11 for tensile specimen in the cap region, C2, and in Figure 12 for tensile specimen close to the root of the weld, R2. The uniform gage section is indicated with the white arrows and the DIC analysis was performed on the white box area, shown on the initial images prior to the tensile loading. The DIC analysis was 2D without resolution in the out of plane direction. It is noted that in the strain maps shown in Figure 11 and Figure 12, the spatial resolution is about 1.3mm, therefore, the highly localized strain at a length scale of less than 1mm cannot be resolved. It is also noted that, the specimens are cylindrical shape, and the measurement resolution has slight error due to depth of the field for 2D analysis.

At 5% of global elongation across the 2-inch (50.8mm) gage section, the two specimen showed stresses (Figure 9), however, the strain maps clearly show the nonuniform deformation of both specimens. Tensile deformation for specimen R2 is mainly outside the weld zone, whereas both base metal and the fusion zone show higher tensile strain for specimen C2. It is noted the highest strain in specimen C2 are localized inside the weld. The heat affected zones (HAZ) of both specimens showed smallest tensile deformation. With increasing tensile deformation to 10% and 15%, the nonuniformity of the tensile deformation across the weld persisted for both specimens. It is noted that the highest tensile strain for C2 remained to be within the fusion zone till failure, whereas the base metal region in R2 experienced large tensile deformation for specimen R2 although the failure location were both within the fusion zone, shown as the highly localized strain at 15% for C2 and 20% for R2.

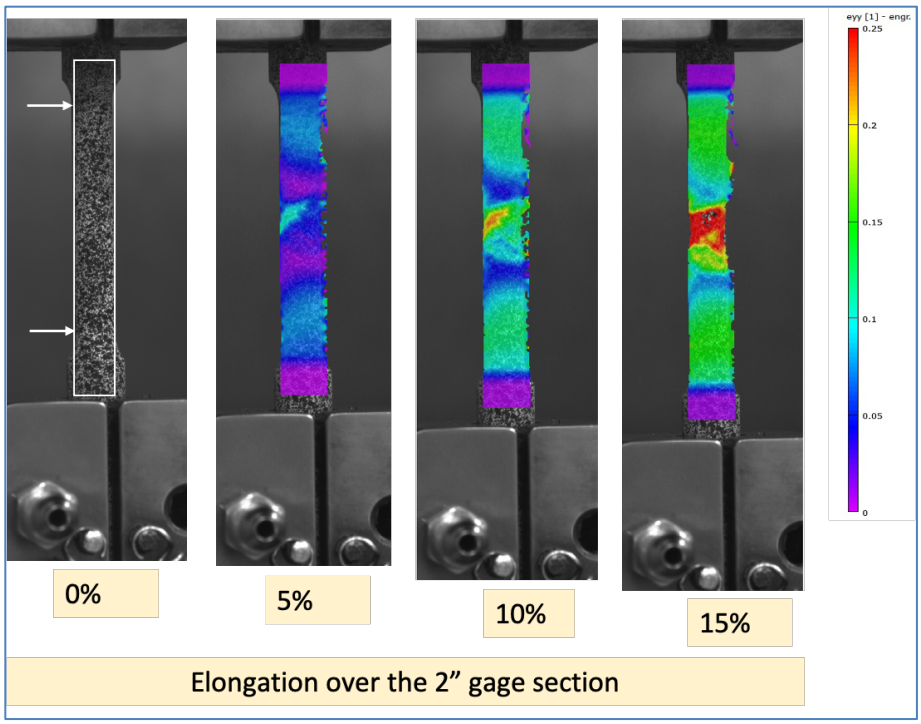

Figure 11. Strain map along tensile direction for specimen C2 (cap of the weld)

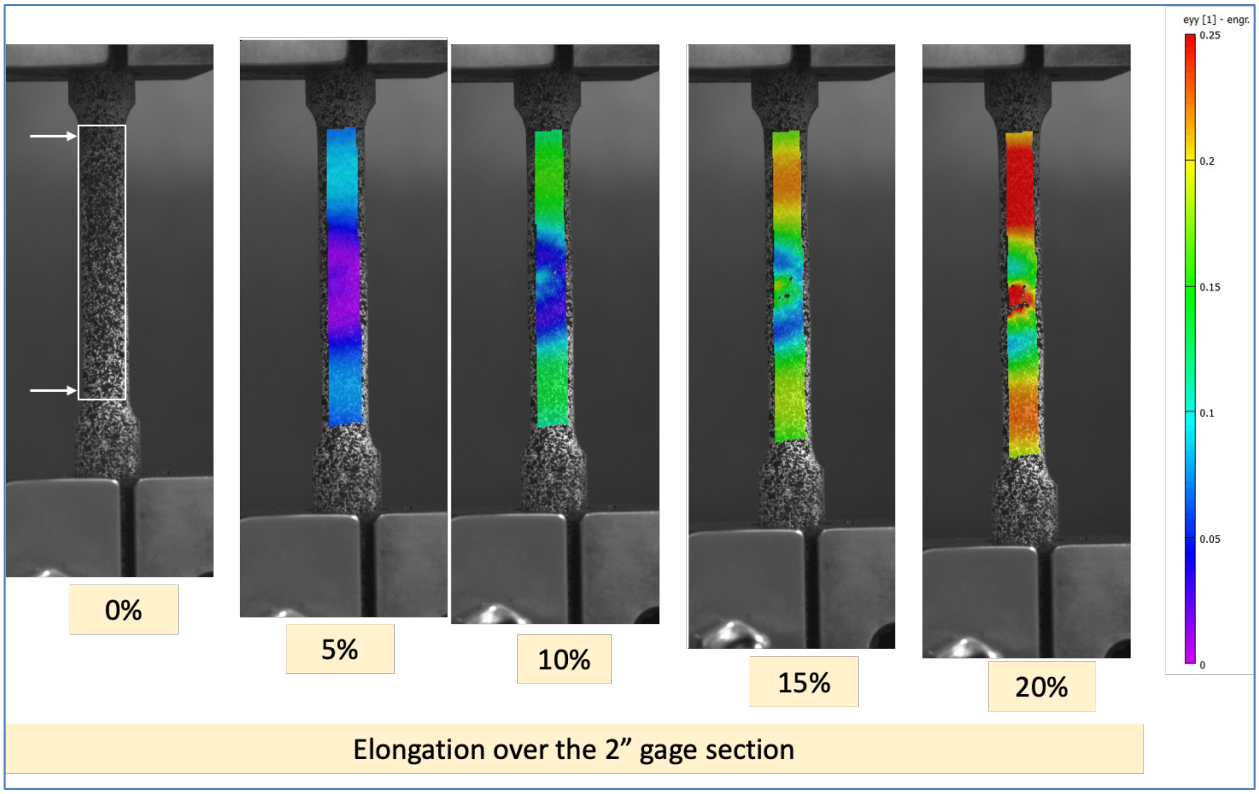

Figure 12. Strain map along tensile direction for specimen R2 (root of the weld)

3.2 MICROSTRUCTURE CHARACTERIZATION OF THE WELD W14

A metallurgical analysis was conducted to characterize the typical microstructures of the weld and its sub-regions, including weld metal (WM) and heat affected zone (HAZ). The optical image in Figure 13 shows the cross-section of the entire weld W14. No obvious weld defects (e.g. porosity, inclusions, or cracks) were observed in this multi-pass weld.

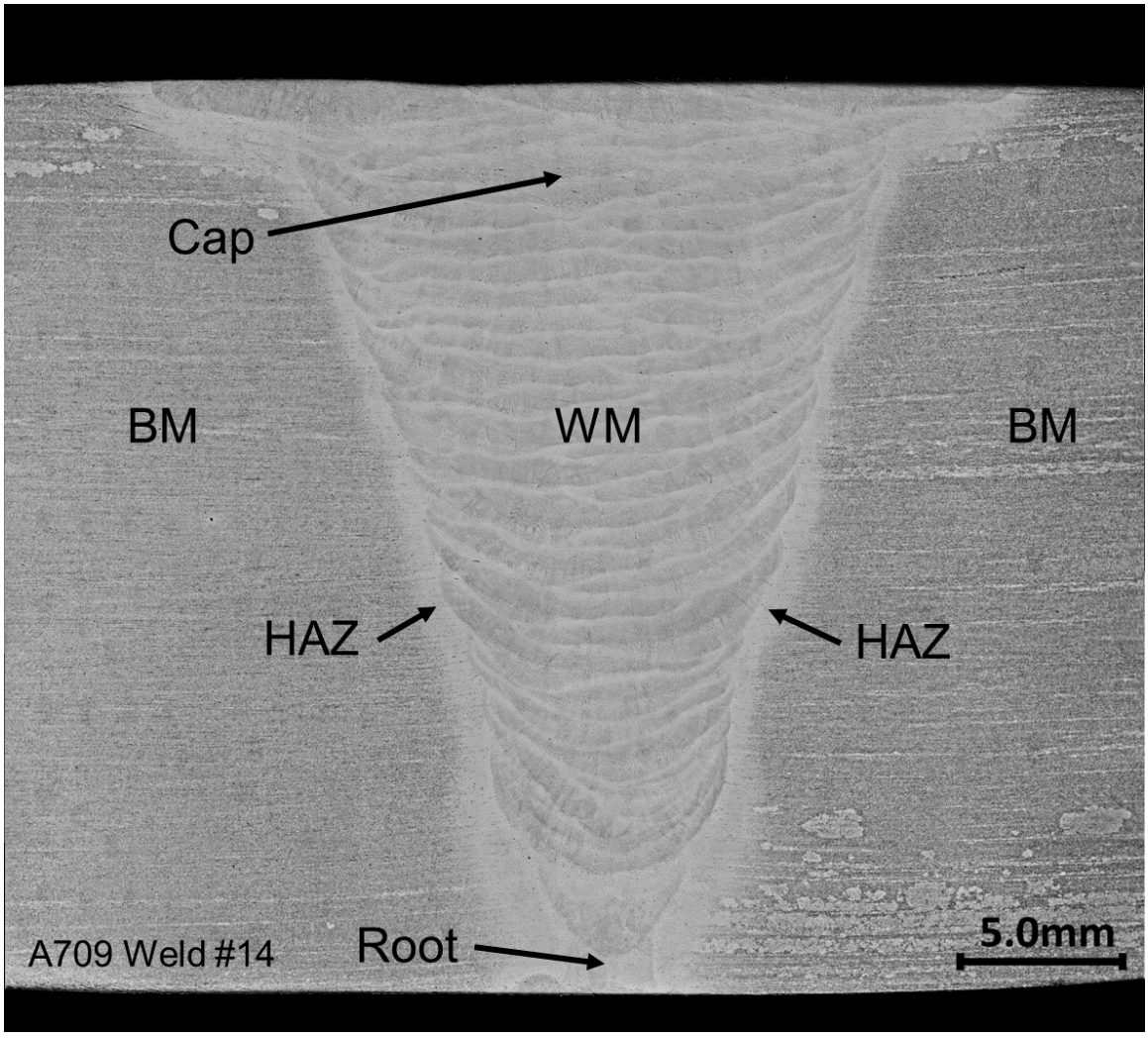

Figure 13. Optical image showing cross-section of the weld W14.
No obvious weld defects or cracks were observed.

Figure 14 presents the typical microstructure of the solidified weld metal without cracks in W14. Figure 14a and Figure 14b show the deposited weld passes in the cap region and root region, respectively. Figure 14c and Figure 14d show the solidified dendrites in the cap weld metal. The dendrites grew perpendicular to the fusion line of each pass. Particles are observed at boundaries of the solidified dendrites (Figure 14d). Backscatter electron SEM images in Figure 15 show the distribution of precipitates inside the solidified dendrites. Those precipitates are likely Nb-rich MX, which nucleated along the dendritic cell boundary during solidification. The cell boundaries are visible, which indicates chemistry differences between the boundaries and cell interiors induced by segregation process during solidification.

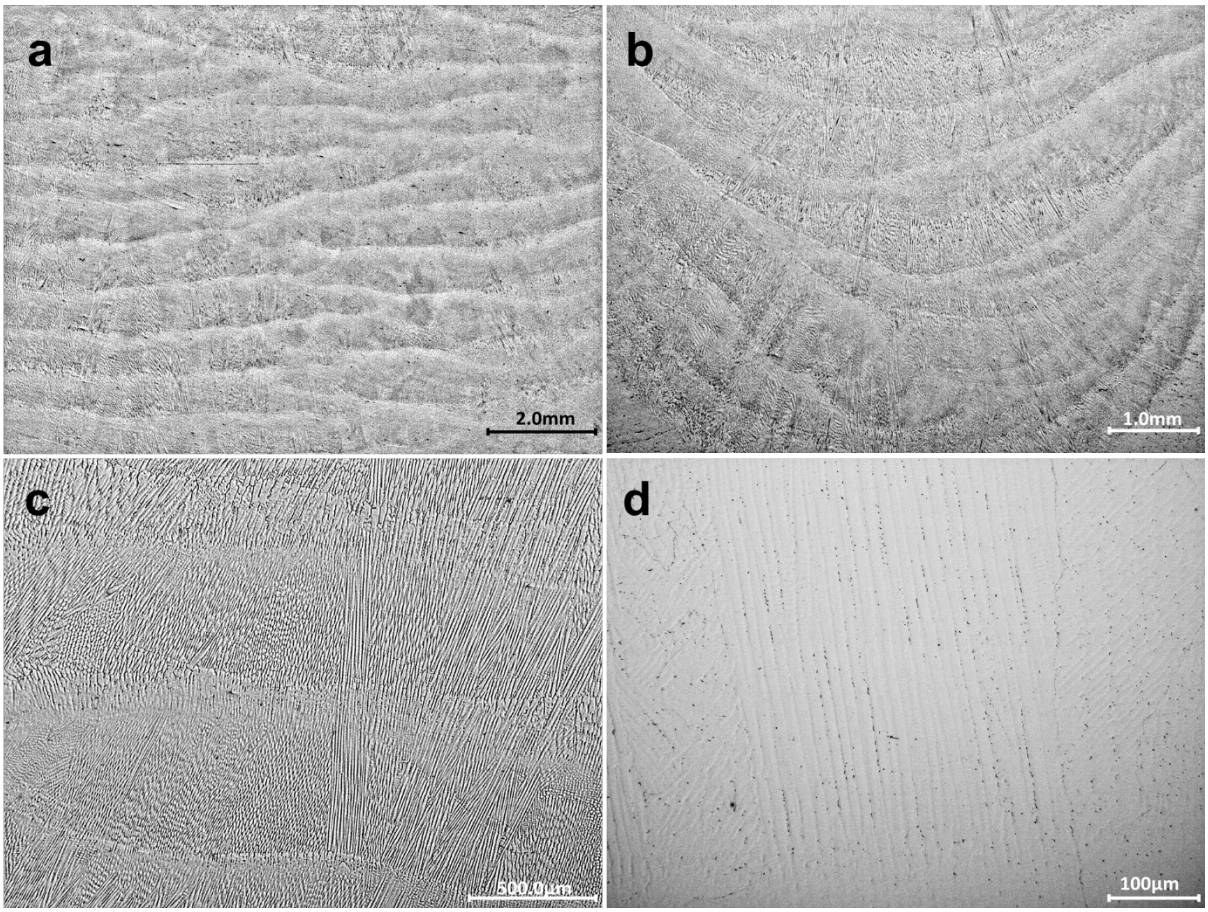

Figure 14. Optical images showing typical microstructure of solidified weld metal for W14. (a) cap region; (b) root region; (c), (d) dendritic microstructure in the cap region.

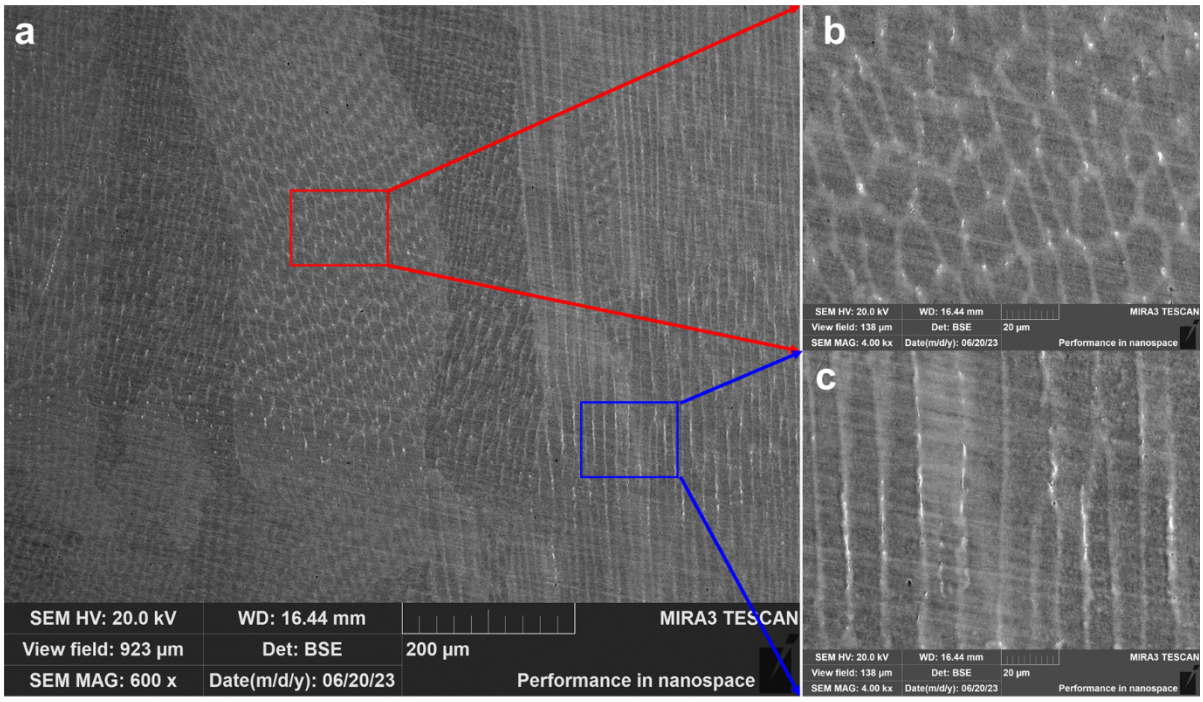

Figure 15. Backscatter election (BSE) SEM images showing precipitates in the solidified dendrites in the cap weld metal for W14

Optical images in Figure 16 show the typical microstructure of heat affected zone (HAZ) in the cap and root regions. The HAZ width in the root region is slightly larger than that in the cap region. An obvious grain growth was observed in the HAZ adjacent to the fusion line due to the high temperature exposure during welding. The welding thermal exposure in HAZ also affected the precipitation behavior near the FL. Figure 17 compares precipitate distributions in the BM and HAZ. Unlike the continuously distributed precipitates (mainly $M_{23}C_6$ carbides) along grain boundaries in the BM, fewer and smaller precipitates are observed in the HAZ (Figure 17b). This indicates the welding thermal exposure caused a precipitation dissolution in the HAZ adjacent to the FL. Large NbC particles are observed in the HAZ due to their higher thermal stability. Meanwhile a cluster of small NbC carbides are observed which indicates dissolution effect from the welding also affected.

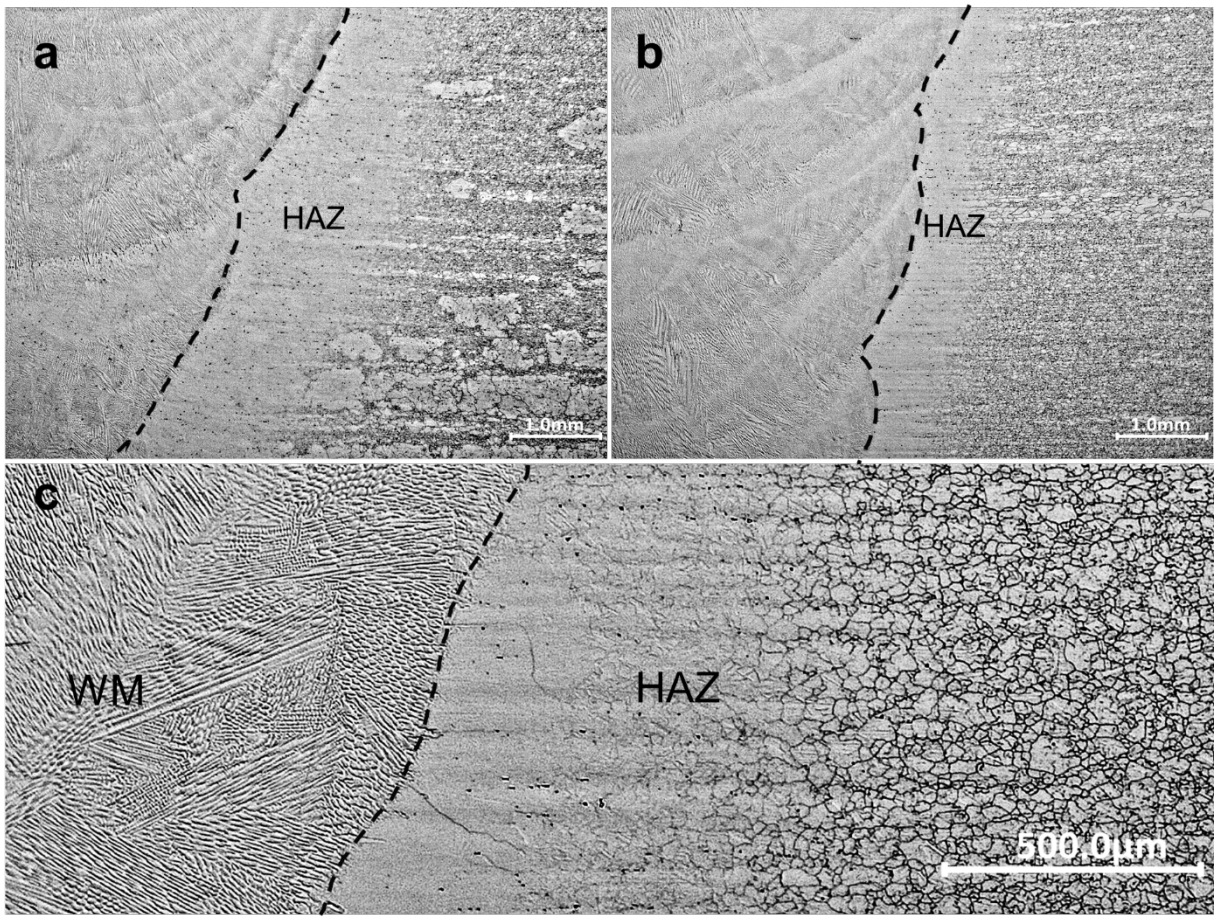

Figure 16. Optical images showing typical microstructure of HAZ near the fusion line (FL) of W14

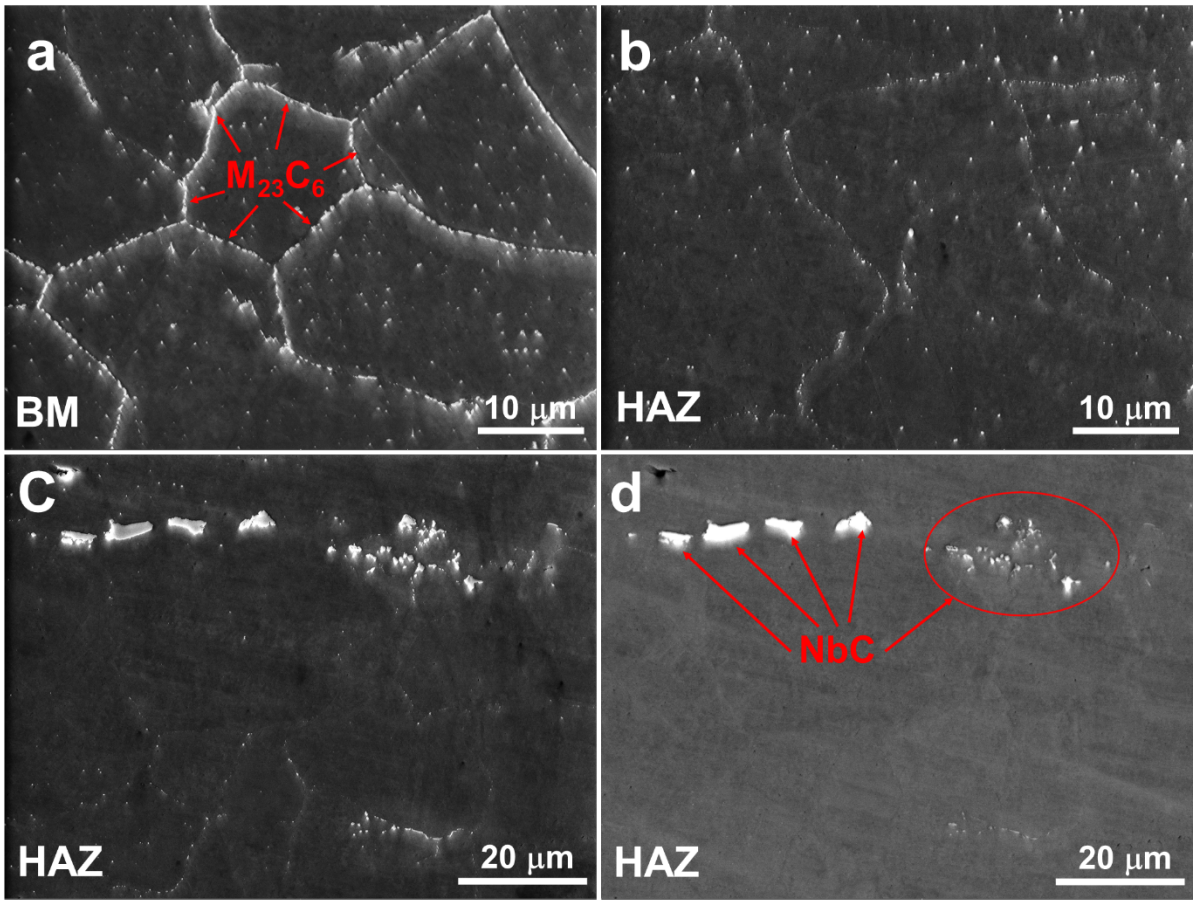

Figure 17. SEM images showing precipitates in the BM and HAZ near the fusion line (FL) of W14. (a) BM; (b), (c), (d) HAZ. (a)-(c) secondary electron images; (d) backscatter electron images

3.2.1 Hardness measurements of the production weld W14

Hardness measurements (line scans and mapping) was conducted to investigate hardness distributions in this complex multi-pass weld. Figure 18 shows multiple microhardness line profile across the cross-section of the weld. Overall, the WM has a higher hardness (250-290 HV0.5) than the hardness (~ 200 HV0.5) of BM, except the WM in the cap region near the very top free surface. HAZ also has a hardness increase up to 295 HV0.5, compared with the BM. These hardness line profiles also present the hardness variations in WM and HAZ along the plate thickness direction. For the WM, its hardness decreased from 290 HV0.5 in the root region to 250 HV0.5 in the cap region. For the HAZ, the hardness gradient decreased along the thickness direction from the root to cap. The HAZ near the root region has a sharp hardness transition while this hardness transition is relatively shallow in the cap region. These hardness heterogeneities are believed to be closely induced by the microstructure inhomogeneities and nonuniform stress levels resulting from the welding process.

Hardness line profile in Figure 19 and optical images of indents in Figure 20 present the hardness values and the evidence of grain growth and precipitate dissolution in the HAZ near the FL. A gradual hardness increase is observed from the FL (236 HV0.5) towards the HAZ on the left (max. 276 HV0.5). The low hardness (232 HV0.5 and 236 HV0.5) of WM (Figure 20h and Figure 20i) and insufficient precipitation strengthening. The faster gain growth and a high degree of precipitate dissolution in the HAZ (0.45mm

distance from the FL) led to a lower hardness than that of the HAZ beyond the 0.45 mm distance from the FL. Figure 21 shows the hardness distribution in the HAZ which is 3.5-4.0 mm away from the FL. There is a hardened HAZ region with high hardness (~ 270-290 HV0.5). This HAZ with different microstructure and hardness may lead to different degradation paths during high temperature service exposure. More in-depth studies may be needed to further investigate their microstructure evolution mechanisms and its corresponding effect on strength reduction at elevated temperatures.

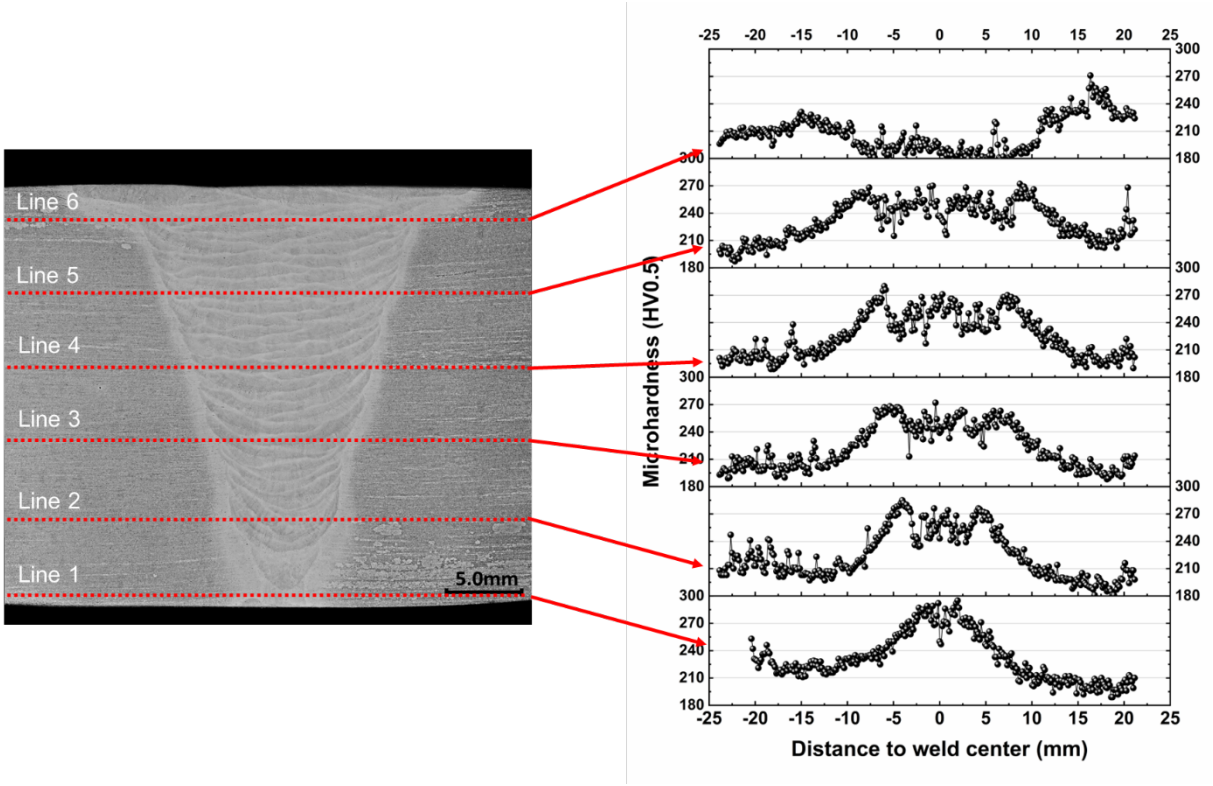

Figure 18. Micorhardness distributions across the cross-section of the weld W14

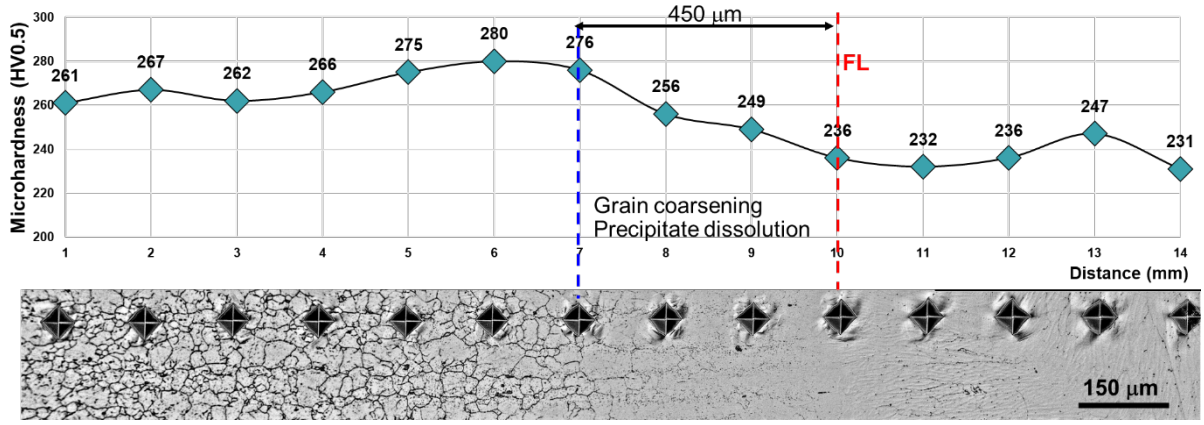

Figure 19. Microhardness profile (from Line 4) and optical image of the HAZ near the fusion line of weld W14.

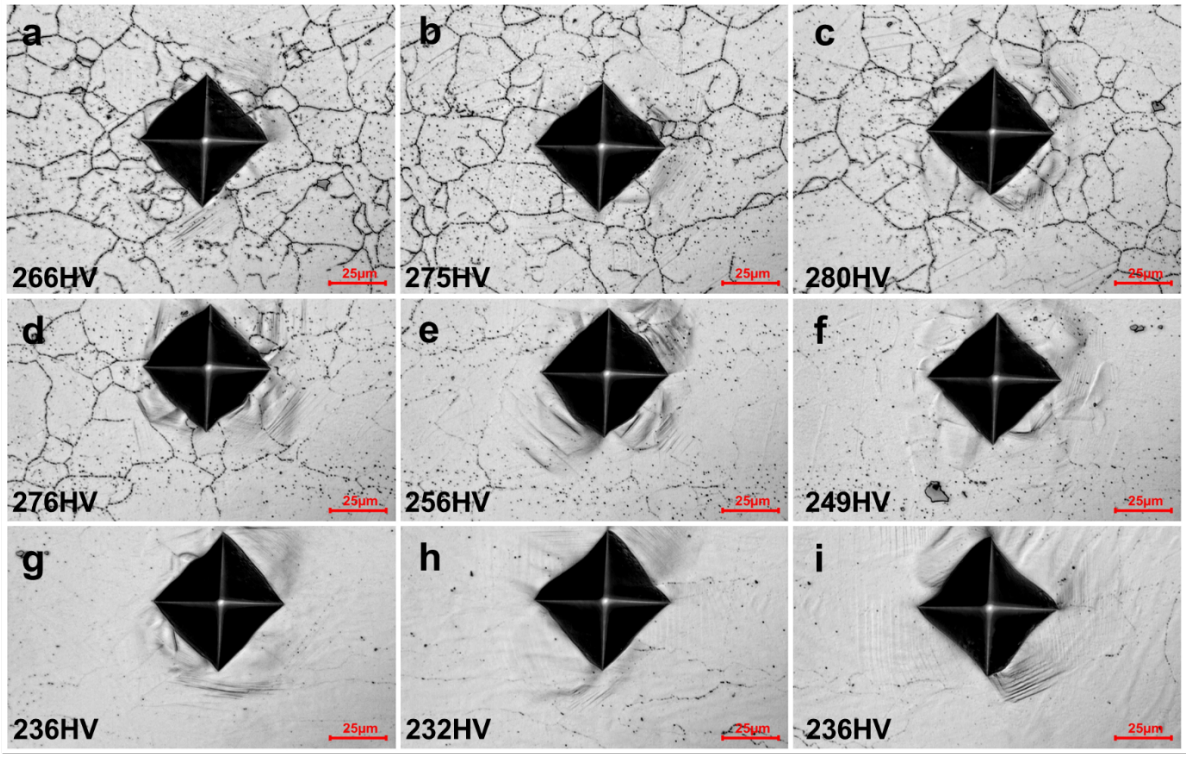

Figure 20. Optical images showing tyical hardness indent and microstrcutureof the HAZ near the fusion line. (a)-(c) HAZ without obvious grain growth and precipitate dissolution; (d)-(f) HAZ with obvious grain growth and precipitate dissolution. (g)-(i) FL towards the WM.

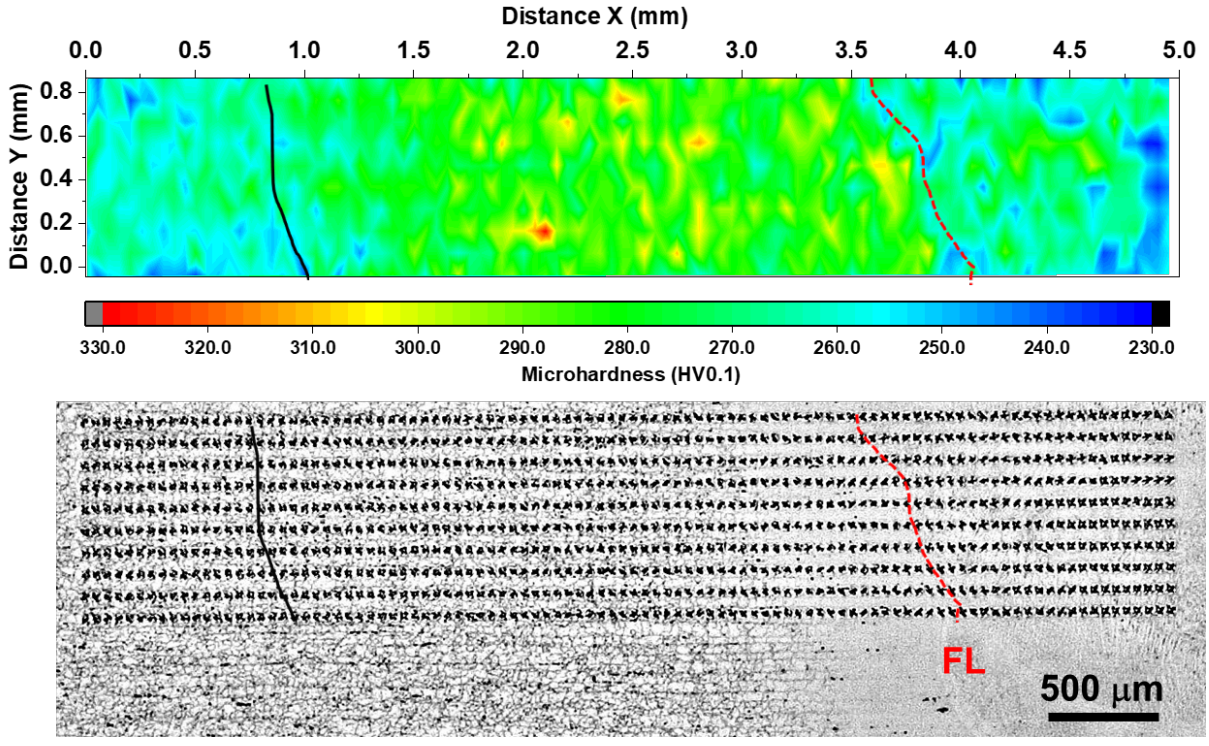

Figure 21. Hardness mapping showing tyical hardness distribution in the HAZ near the fusion line

4. PRELIMINARY CREEP TEST RESULTS ON ALLOY 709 WELDS

These two production welds, W10 and W11, were fabricated on the two commercial heats of A709 plates using A709 filler metal with P content less than 20 wppm. W10 was fabricated on Carlson heat 58776, plate 58776-3RBC1 with 1.1-inch thickness, and W11 was fabricated on ATI heat 529900, plate CG05454 with 2.05-inch thickness. The detailed weld fabrication parameters and qualification tests on these two production welds were reported in Feng, et al. (2022). Cross-weld creep rupture Code Case testing on the production weld W11 was initiated.

Creep testing of the Alloy 709 weld W6, the same welding parameters and material as W10 continued. Table 6 lists the creep testing parameters and the updated status of the test welds as well as the production welds. In this table, the weld identification numbers are consistent with the previous report in Feng et al. (2019, 2020, 2021, 2022). The results from the preliminary creep tests are used to develop the creep testing matrix for the more comprehensive creep testing on Alloy 709 weds in support of the development of the Alloy 709 Code Case data package.

For comparison purposes, the Larson-Miller relationship was used to compare all the available creep rupture results on the Alloy 709 welds with the rupture data generated on the two commercial heats of Alloy 709 base metal in precipitation treatment condition (PT condition) shown in Sham et al., 2022. The results are presented in Figure 22. In this plot, the Larson-Miller parameter (LMP) was based on Eq. (1):

$$LMP = (T + 273.15) * (16.6958 + \log t_r), \quad (1)$$

where T is temperature in degrees Celsius and t_r is rupture life in hours, and C is a constant.

This preliminary analysis indicates that the ATI heat 529900 with PT condition has slightly higher creep strength than the Carlson heat 58776 with PT condition.

From the limited preliminary creep rupture data on weld W2, W5 and W6 and the comparisons with the base metal, the rupture life of Alloy 709 cross-welds continued to show little or no reduction in their creep strength. It is noted that tests at high stress of 330MPa at 600°C are omitted in this analysis due to the large loading strain beyond the yield.

The creep testing matrix for the production weld are developed, and the results will be used to establish the stress rupture factors for Alloy 709. Additional creep rupture Code Case testing of the production weld W10 and W11 will be performed when creep frames are open, and resources are available in FY 2024.

Table 6. Cross-weld creep testing of Alloy 709 welds

ID	Weld wire and base metal plates	Test number	Temp (ºC)	Stress (MPa)	Rupture time, (hr)
W2	**Weld wire heat#:** 011367-08 with P < 20 wppm; **Base meatal heat#:** 58776-3R with P content of 140 wppm	34276*	600	330	602.7
		34325*	600	330	378
		34455*	600	330	353
		34456	925	27	342
		34458	775	80	2300
W5	**Weld wire heat#:** 58776-4A with P content of 140 wppm; **Base meatal heat#:** 58776-3R with P content of 140 wppm	38440*	600	330	6.5
		38439	650	175	5,092.2
		38468	625	175	15940
		38467	650	150	15254.4
		38469	775	80	2464.5
W6	**Weld wire heat#:** 011367-08 with P< 20 wppm; **Base meatal heat#:** 58776-3RB with P content of 140 wppm**;** heat treated at 775 °C for 10 h	40014	750	100	2336
		40017	800	50	6055.7
		40980	800	35	Ongoing, >13,300 hr
		41185	725	75	Ongoing, >12,500 hr
		41186	700	93	Ongoing, >12,500 hr
W11	**Weld wire heat#:** 011367-08 with P< 20 wppm; **Base meatal heat#:** 529900, with P content of 30 wppm**;** heat treated at 775 °C for 10 h	43112	975	15	Ongoing
		43113	1000	11	Ongoing
		43096	975	17	Ongoing
		43111	975	13	Ongoing

Note: *These tests are excluded for creep strength evaluation due to the large loading strain beyond yield and evidence of welding defect in this specimen.

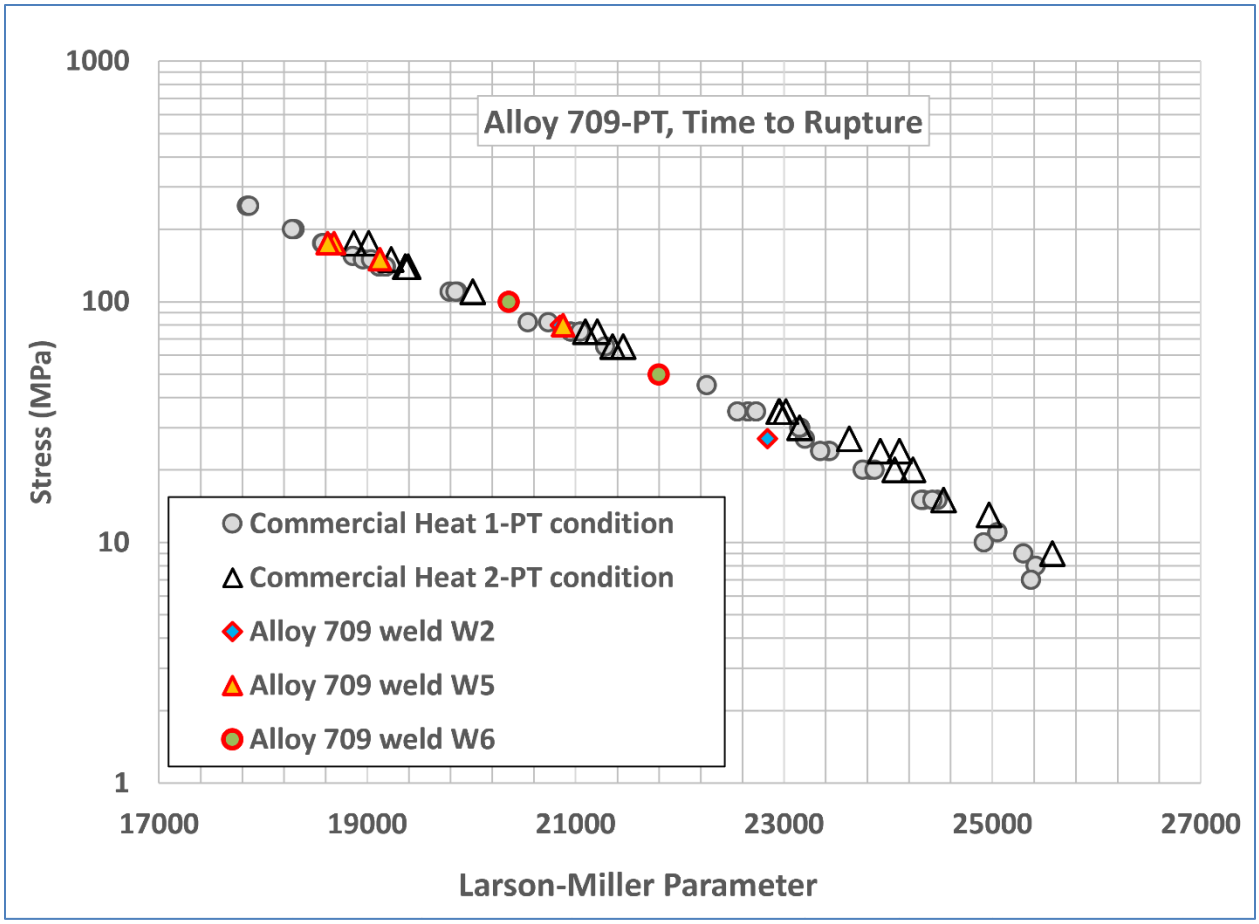

Figure 22. Comparison of creep rupture testing results of Alloy 709 welds and base metal in PT condition.

5. SUMMARY AND FUTURE PLAN

This report summarizes the Alloy 709 (A709) welding research conducted in FY 2023 at ORNL. A new A709 weld wire was processed from the ATI heat No. 530843, plate CG45192 with 80 wppm of P through a wire cold drawing process. This weld wire was used to fabricate W14 weld on the high P containing Carlson heat plate with GTAW process. This weld passed all weld qualification tests without issues. This study concludes that the P content in the A709 weld wire can be relaxed to 80 wppm.

The research on Alloy 709 weldability in this program so far supports the strategy for successfully welding Alloy 709 having wide range of chemistries without weld solidification cracking.

The cross-weld creep rupture Code Case testing was initiated on the A709 production welds. The preliminary creep tests results continue to show little or no creep strength reduction relative to the base metal.

6. BIBLIOGRAPHY

ASME. (2019). *Qualification Standard for Welding, Brazing, and Fusing Procedures; Welders; Brazers; and Welding, Brazing, and Fusing Operators.* ASME Boiler and Pressure Code.

ASME. (2021). *Specification for seamless ferritic and austenitic alloy-steel boiler, superheater, and heat-exchanger tubes.* ASME Boiler and Pressure Code, 2021 Edition.

ASTM International. (2018). *E139-11 Standard Test Methods for Conducting Creep, Creep-Rupture, and Stress- Rupture Tests of Metallic Materials*. Retrieved from www.astm.org.

ASTM International. (2022). *E8-2022, Standard Test Methods for Tension Testing of Metallic Materials.* Retrieved from www.astm.org

Busby, J. T., Byun, S., Klueh, R., Maziasz, P., Vitek, J. M., Natesan, K., . . . Allen, T. (2008). *Candidate Developmental Alloys for Improved Structural Materials for Fast Reactors.* ORNL/GNEP/LTR-2008-023, Oak Ridge National Laboratory, Oak Ridge, TN.

Feng, Z., Dai, T., Kyle, D., Wang, Y., & Wang, Y. (2020). *Welding Parameters Optimization and the Fabrication of Qualified Alloy 709 Welds.* ORNL/TM-2020/1706, Oak Ridge National Labaratory, Oak Ridge, TN.

Feng, Z., Dai, T., Kyle, D., Wang, Y., & Wang, Y. (2021). *Report on FY 2021 Fabrication and Testing of Qualified Alloy 709 Welds at ORNL.* ORNL/TM-2021/2171, Oak Ridge National Laboratory, Oak Ridge, TN.

Feng, Z., Vitek, J. M., Liu, T., & Wang, Y. (2018). *Evaluation of the Effect of Alloy Chemistry on the Susceptibility of Weld Solidification Cracking of Alloy 709 Weldment and Development of Mitigation Strategy.* ORNL/TM-2018/965, Oak Ridge National Laboratory, Oak Ridge, TN.

Feng, Z., Wang, Y., Kyle, D., & Dai, T. (2019). *Report on FY19 Fabrication and Evaluation of Weldment for Alloy 709 Commercial Heat Plates.* ORNL/TM-2019/1320, Oak Ridge National Laboratory, Oak Ridge, TN.

Natesan, Natesan, K., Zhang, X., Sham, T.-L., & Wang, H. (2017). *Report on the completion of the procurement of the first heat of Alloy 709.* ANL-ART-89, Argonne National Laboratory, Lemont, IL.

NIPPON STEEL & SUMITOMO STEEL. (2013). *NF709 Material Data Sheet.* Retrieved from http://www.tubular.nssmc.com/product-services/specialty-tube/product/nf709

Sham, T.-L., & Natesan, K. (2017). Code Qualification Plan for an Advanced Austenitic Stainless Steel, Alloy 709, for Sodium Fast Reactor Structural Applications. *International Conference on Fast Reactors and Related Fuel Cycles*, (pp. IAEA-CN-245-74). Yekaterinburg, Russian Federation.

Siefert, J., & David, S. A. (2014). Weldability and weld performance of candidate austenitic alloys for advanced ultrasupercritical fossil power plants, Science and Technology of Welding and Joining, 19:4, 271-294. *Sci Tech Welding Joining, 19*(4), 271-294.

Van Wortel, H. (2007). Control of relaxation cracking in austenitic high temperature components. *NACE Corrosion Conf. Expo.* (p. Paper 07423). Houston, TX: NACE International.

Wu, Z., Penso, J., Chen, T., Leonard, D. N., Zhang, D., David, S. A., & Feng, Z. (2020). Microstructural examination of a 347H austenitic stainless steel weld after 30-years' refinery service. *ASME Pressure Vessels & Piping Conference*, (pp. PVP2020- 21641).

Yamamoto, Y. (2014). Unpublished data. Oak Ridge National Laboratory.

Zhang, X., Sham, T.-L., & Young, G. A. (2019). *Microstructural Characterization of Alloy 709 Plate Materials with Additional Heat Treatment Protocol.* ANL-ART-170, Argonne National Laboratory, Lemont, IL.